Title: The quantitative studies on gas explosion suppression by an inert rock dust deposit

Authors: Yifan Song, Qi Zhang

PII: S0304-3894(18)30213-9
DOI: https://doi.org/10.1016/j.jhazmat.2018.03.052
Reference: HAZMAT 19272

To appear in: *Journal of Hazardous Materials*

Received date: 29-9-2017
Revised date: 25-3-2018
Accepted date: 27-3-2018

Please cite this article as: Song Y, Zhang Q, The quantitative studies on gas explosion suppression by an inert rock dust deposit, *Journal of Hazardous Materials* (2010), https://doi.org/10.1016/j.jhazmat.2018.03.052

The quantitative studies on gas explosion suppression by an inert rock dust deposit

Yifan Song, Qi Zhang*

State Key Laboratory of Explosion Science and Technology, Beijing Institute of Technology, Beijing 100081, China

* Corresponding author. Tel./fax: +86 10 68914252.
E-mail address: qzhang@bit.edu.cn (Q. Zhang).

Highlights:

- The process of the rock dust cloud barrier forming is demonstrated.
- The characteristics of the explosion field at different deposited rock dust amounts are investigated.
- The lower limit of the deposited inert rock dust amount is researched.
- The suppression effects begin to weaken when the deposited rock dust amount increases to a certain value.

Abstract: The traditional defence against propagating gas explosions is the application of dry rock dust, but not much quantitative study on explosion suppression of rock dust has been made. Based on the theories of fluid dynamics and combustion, a simulated study on the propagation of premixed gas explosion suppressed by deposited inert rock dust layer is carried out. The characteristics of the explosion field (overpressure, temperature, flame speed and combustion rate) at different deposited rock dust amounts are investigated. The flame in the pipeline cannot be extinguished when the deposited rock dust amount is less than 12 kg/m^3. The effects of suppressing gas explosion become weak when the deposited rock dust amount is greater than 45 kg/m^3. The overpressure decreases with the increase of the deposited rock dust amounts in the range of 18-36 kg/m^3 and the flame speed and the flame length show the same trends. When the deposited rock dust amount is 36 kg/m^3, the overpressure can be reduced by 40%, the peak flame speed by 50%, and the flame length by 42% respectively, compared with those of the gas explosion of stoichiometric mixture. In this model, the effective raised dust concentrations to suppress explosion are 2.5-3.5 kg/m^3.

Keywords: Deposited rock dust; Overpressure; Temperature; Flame speed; Flame length

1. Introduction

As the quantity of gas extraction in coal mines having increased year by year in China, great potential safety hazard exists in the process of long-distance pipeline transportation [1]. In recent years, mine gas explosion accidents occur occasionally in China. Explosion suppression by inert dust is a common method used to prevent such accidents [2]. However, owing to the complicated interactions and reactions of the gas-solid two-phase flow, the mechanism and the effect of suppressing explosion with inert dust have not been systematically examined, and the inert dust explosion suppression systems are designed with a certain degree of blindness.

A large number of experimental investigations have been made on explosion suppression. Gieras et al. experimentally studied the effect of $NaHCO_3$ suppression on gas and dust explosion in the 5 L vessel [3]. Wang et al. produced a new kind of economical explosion suppression powders, the $NaHCO_3$ /red-mud (RM) composite powders, which displayed a much better suppression property than the pure RM or $NaHCO_3$ powders [4]. Chen et al. performed explosion tests for gas flame suppression by SiO_2 powder and found that the superfine SiO_2 powder can reduce the explosion peak pressure and flame speed by more than 40% [5]. Amrogowic et al. compared the suppression effects of $NaHCO_3$ and $(NH_4)H_2PO_4$ and concluded that $(NH_4)H_2PO_4$ was better than $NaHCO_3$ in deactivation, but $NaHCO_3$ was more effective in suppressing explosion [6]. In addition, the powder suppressant can effectively constraint the explosion pressure and flame, and can suppress the secondary explosions under the coal mine [7].

Moreover, simulations based on Computational Fluid Dynamics (CFD) have been applied widely to study complex fluid flow problems, including gas and dust explosion processes [8, 9], explosion venting process [10, 11], dust lifting process [12, 13] and turbulent fluid flow process [14]. In addition, some researchers have studied the microscopic effects and scale effects in the process of powder explosion suppression with numerical simulations. Kosinski numerically studied the progress of solid particles suppression explosion [15]. Oleszczak et al. [16], Krasnyansky et al. [17] and Klemens et al. [18] conducted a large number of simulation investigations to scrutinize the explosion processes and the control processes and found that the main contributing factors of explosion suppression included particle types, particle concentrations, particle diameters and particles dispersion states, et cetera.

At present, most researchers carry out experimental studies on explosion suppression under static conditions which intends inhibitor is in the ideal state of uniform diffusion from the beginning. Furthermore, the

experimental systems are usually small vessels and pipes [19-21]. The studies on the effect of dry dust explosion suppression and its influencing factors in the dynamic propagation state, if there are any, are not presented in the literature. Explosion suppression of inert rock dust at various concentrations, reaction between explosion flame and the raised rock dust particles, and local concentration of the suspended dust are the bases for design of explosion suppression. However, the related literature has not been available. It is difficult to examine lifting mechanism of dust particles behind an explosion wave, especially reaction between explosion flame and the raised rock dust particles in experiments. In this study, the mathematical model of a turbulent explosion of combustible gas in pipeline has been built up to scrutinize the dynamic process of explosion suppression by inert rock dust. The objectives are to unravel the interaction mechanism of inert dust with flame and shock wave, and to find the limits of inert dust amounts to the effective explosion suppression. In addition, this study can provide a basis for the calculation of key parameters and the control measures for explosion accidents of combustible gas.

2. Physical and mathematical models

2.1. Governing equations

In this study, the governing equations of the gas phase flow are the Navier-Stokes equations (1)-(4); turbulence model used in the calculation is the standard k-ε model based on turbulence kinetic energy and diffusion rate, equations (5)-(8); combustion model used is the finite-rate/eddy-dissipation model, equations (9)-(12). The discrete phase model (DPM) is used to solve the trajectories of dust particles by integrating differential equations (13)-(17) of the particle force in the integral coordinate. The discrete phase model (DPM) follows the Euler-Lagrange approach [22, 23]. The fluid phase is treated as a continuum by solving the time-averaged Navier-Stokes equations, while the dispersed phase is solved by tracking a large number of particles through the calculated flow field. The dispersed phase can exchange momentum, mass, and energy with the fluid phase. It is to note that gas explosion and suppression in the pipeline is a complex physical and chemical process. Therefore, the interactions among particles as well as forces acting on the wall are ignored to reasonably simplify the model [24]. The heat transfer from the continuous phase to the discrete phase is computed by equation (18).

The mass conservation equation is:

$$\frac{\partial \rho}{\partial t}+\frac{\partial}{\partial x_j}\left(\rho u_j\right)=0 \tag{1}$$

The momentum conservation equation is:

$$\frac{\partial}{\partial t}(\rho u_i)+\frac{\partial}{\partial x_j}(\rho u_j u_i)=-\frac{\partial p}{\partial x_i}+\frac{\partial \tau_{ij}}{\partial x_j} \tag{2}$$

where

$$\tau_{ij}=\left[\mu\left(\frac{\partial u_i}{\partial x_j}+\frac{\partial u_j}{\partial x_i}\right)\right]-\frac{2}{3}\mu\frac{\partial u_i}{\partial x_i}p_{ij} \tag{3}$$

The energy conservation equation is:

$$\frac{\partial}{\partial t}(\rho E)+\frac{\partial}{\partial x_i}[u_i(\rho E+p)]=\frac{\partial}{\partial x_i}\left[\kappa_{eff}\frac{\partial T}{\partial x_i}-\sum_{j'}h_{j'}\vec{J}_{j'}+u_j(\tau_{ij})_{eff}\right]+S_h \tag{4}$$

where ρ is the density, kg/m^3; x the space coordinate, m; t the time coordinate, s; u the velocity, m/s; i and j the coordinate directions; p the static pressure, Pa; τ_{ij} the viscous stress tensor, kg/ m·s^2; μ the turbulence viscosity, N·s/m^2; κ_{eff} the effective thermal conductivity, W/m·K; h the sensible enthalpy of compressible gases, kJ/mol; and S_h is the source term of chemical reaction energy, W/m^3.

k equation is:

$$\frac{\partial}{\partial x_i}(\rho k u_i)=\frac{\partial}{\partial x_j}\left[\left(\mu+\frac{\mu_t}{\sigma_k}\right)\frac{\partial k}{\partial x_j}\right]+G_k-\rho\varepsilon \tag{5}$$

ε equation is:

$$\frac{\partial}{\partial x_i}(\rho\varepsilon u_i)=\frac{\partial}{\partial x_j}\left[\left(\mu+\frac{\mu_t}{\sigma_\varepsilon}\right)\frac{\partial \varepsilon}{\partial x_j}\right]+C_1\frac{\varepsilon}{k}G_k-C_2\rho\frac{\varepsilon^2}{k} \tag{6}$$

where

$$\mu_t=C_\mu\rho\frac{k^2}{\varepsilon} \tag{7}$$

$$G_k=\mu_t\left(\frac{\partial u_i}{\partial x_i}+\frac{\partial u_j}{\partial x_j}\right)\frac{\partial u_i}{\partial x_j} \tag{8}$$

where u_i , u_j are the velocities along x, y axis respectively, m/s ; μ_t the turbulent viscosity coefficient, Pas; G_k the shear force caused by the fluctuation of turbulent kinetic energy rate ,kg/ m· s^3; k the turbulent kinetic energy, m^2/s^2 ; ε the turbulent dissipation rate, m^2/s^3; and C_1 , C_2 , C_μ , σ_k and σ_ε are all the constant in this model. The values are assigned according to Launder [25]: C_1 = 1.44, C_2 =1.92, C_μ =0.09, σ_k =1.0, σ_ε

=1.3.

The reaction rates that appear as source terms in Equation (4) are computed by finite-rate/eddy-dissipation model, where both the Arrhenius (Equation (10)), and eddy-dissipation (Equations (11) and (12)) reaction rates are calculated. The net reaction rate is taken as the minimum of these two rates. The net source of chemical species i due to reaction is computed as the sum of the Arrhenius reaction sources over the N_R reactions that the species participate in:

$$R_i = M_{w,i} \sum_{r=1}^{N_R} \hat{R}_{i,r} \tag{9}$$

where $M_{w,i}$ is the molecular weight of species i and $\hat{R}_{i,r}$ is the Arrhenius molar rate of creation/destruction of species i in reaction r.

The molar rate of creation/destruction of species i in reaction r is given by

$$\hat{R}_{i,r} = \left(v''_{i,r} - v'_{i,r}\right)\left(k_{f,r} \prod_{j=1}^{N} \left[C_{j,r}\right]^{\left(\eta''_{j,r} + \eta'_{j,r}\right)}\right) \tag{10}$$

where $v''_{i,r}$ is the stoichiometric coefficient for product i in reaction r; $v'_{i,r}$ the stoichiometric coefficient for reactant i in reaction r; $k_{f,r}$ the forward rate constant for reaction r; N the number of chemical species in the system; $C_{j,r}$ the molar concentration of species j in reaction r, kg·mol/m^3; $\eta''_{j,r}$ the rate exponent for product species j in reaction r; and $\eta'_{j,r}$ is the rate exponent for reactant species j in reaction r.

The eddy-dissipation model is a turbulence-chemistry interaction model [26]. The net rate of production of species i due to reaction r, $R_{i,r}$, is given by the smaller of the two expressions below:

$$R_{i,r} = v'_{i,r} M_{w,i} A \rho \frac{\varepsilon}{k} \min_R \left(\frac{Y_R}{v'_{R,r} M_{w,R}}\right) \tag{11}$$

$$R_{i,r} = v'_{i,r} M_{w,i} A B \rho \frac{\varepsilon}{k} \frac{\sum_P Y_P}{\sum_j^N v''_{j,r} M_{w,j}} \tag{12}$$

where Y_R is the mass fraction of any reactant species R; Y_P the mass fraction of any product species P; A an empirical constant equal to 4.0; and B is an empirical constant equal to 4.0. In Equations (11) and (12), the chemical reaction rate is governed by the large eddy mixing time scale, $\frac{\varepsilon}{k}$; combustion proceeds whenever

turbulence is present ($\frac{\varepsilon}{k} > 0$), and an ignition source is not required to initiate combustion.

The force equilibrium equation of dust particle phase is:

$$\frac{du_p}{dt} = F_D(u - u_p) + \frac{g_x(\rho_p - \rho)}{p_p} + F_x \tag{13}$$

where

$$F_D\left(u - u_p\right) = \frac{18\mu}{\rho_p d_p^2}\frac{C_D Re}{24}\left(u - u_p\right)d_p \tag{14}$$

$$Re = \frac{\rho d_p \left|u_p - u\right|}{\mu} \tag{15}$$

$$\begin{cases} C_D = \dfrac{24}{Re}(1 + 0.15Re^{0.687})(Re < 800) \\ C_D = \dfrac{19.65}{Re^{0.633}}\left(5 < Re < 100\right) \end{cases} \tag{16}$$

$$F_X = \frac{1}{2}\frac{\rho}{\rho_p}\frac{d}{dt}(u - u_p) \tag{17}$$

where u_p is the velocity of particles, m/s; F_D the drag force acting on the particles, N; ρ_p the density of particles, kg/m^3; d_p the particle diameter, m; F_x the other forces acting on particles, N; C_D the drag coefficient, dimensionless; and Re is the Reynolds number, dimensionless.

The study uses a simple heat balance to relate the particle temperature, $T\left(t\right)_p$, to the convective heat transfer and the absorption/emission of radiation at the particle surface:

$$m_p c_p \frac{dT_p}{dt} = \hbar A_p\left(T_\infty - T_p\right) + \varepsilon_p A_p \sigma\left(\theta_R^4 - T_p^4\right) \tag{18}$$

where m_p is the mass of the particle, kg; c_p the heat capacity of the particle, J/kg·K; A_p the surface area of the particle, m^2; T_∞ the local temperature of the continuous phase, K; $\hbar$ the convective heat transfer coefficient, W/m^2·K; ε_p the particle emissivity, dimensionless; σ the Stefan-Boltzmann constant, 5.67$\times$10^{-8} W/m^2·K; and θ_R is the radiation temperature, K.

2.2. Physical model

The simplified two-dimensional model is a large scaled pipeline with a length of 398 m and a height of 2.68 m, as

shown in Fig. 1. One side of the pipeline is assumed closed, while the other side is opened to the atmosphere. On the side of the closed end, a 28 m long section is filled with a homogeneously premixed gas (with methane volume content at 9.5%). A spark ignition region is placed near the closed end. The inert dust particles are layered homogeneously on the bottom of the pipeline, and the inert dust layer is 300 m long deposited at 30 m from the closed end.

The mesh is shown in Fig. 2. Structured grids are used in conjunction with unstructured grids in the ignition area, and the near-wall grids are densified.

2.3. Parameter settings

In the literature, the experimental inert particles' sizes are on the micrometer scale [27-29]. Referring to the experimental values, the diameter distribution of inert particles is in the range of 5-100 μm, as shown in Table 1. The length of rock dust layer is referred to in the 159th regulations of China's *Coal Mine Safety Regulation* [30]. The dust is deposited in the range of 30-330 m from the closed end. The amounts of deposited rock dust simulated are: 7 kg/m^3, 12 kg/m^3, 18 kg/m^3, 24 kg/m^3, 30 kg/m^3, 36 kg/m^3 and 45 kg/m^3.

Other constant parameters are shown in Table 2.

2.4. Verification of the numerical method

In order to determine the optimal grid density, three models (as shown in Table 3) with the grid resolution of 106 300, 584 800 and 1 154 400 are tested.

Fig. 4 shows the peak overpressures along the pipeline of the premixed methane-air explosion under the three models. The iteration step is set to 5×10^{-5} s. Compared with the experimental results under the same conditions of Xu et al. [31], the relative errors between the experiment and the simulations are 14.2%、5.8% and 4.3%, respectively. The results show that the finer grid density is, the more accurate the simulation result. Fig. 5 shows the maximum explosion pressure rising rates along the pipeline axis under the three models. It is indicated that the rate of pressure rise tends to be stable with mesh refinement, and a finer grid density (Model Ⅲ, 1 154 400 grids) does not yield any significant improvement.

To improve computational efficiency and reduce cost (the CPU is Inter Core i7-7700 clocked at 3.60 GHz), based on the above analysis, Model Ⅱ, consisting of 584 800 grids, is adopted as the simulation model for the explosion suppression of rock dust.

In order to verify the appropriateness of the model parameters, a simulation of the flame propagation of premixed methane-air with rock dust in square tube under experimental conditions [32] is carried out, and the results are shown in Fig. 5. It is apparent that the simulation is able to well represent both the transient places of flame fronts and the average speed of flame propagating. As a result, the model parameters satisfy the simulation requirements of the explosion suppression.

3. Simulation results and analysis

3.1. Peak overpressure and the propagation of rock dust rising

Fig. 6 shows the pressure distribution and the rock dust lifting process. A plane shock wave produced by the premixed gas explosion advances along the pipeline (see Fig. 6 0.015 s). Particles deposited are kicking up at 0.039 s, while the shock wave appears not uniform due to the rock dust blocking. It is clear in Fig. 6 that the deposited rock dust kicking up is induced by the explosion shock wave[33, 34], and consequently a barrier formed by the inert rock dust cloud fills the cross section of the pipeline.

Fig. 7 presents the peak overpressure along the pipeline for different deposited rock dust amounts. With the increase of rock dust amounts, the maximum explosion pressure decreases gradually, therefore laying inert rock dust layer can reduce the damage extent of explosion [35]. When the amount of deposited rock dust reaches 45 kg/m^3, the maximum explosion pressure is greater than that of 36 kg/m^3, indicating that the explosion suppression effect of rock dust is related to the deposited dust amount. This is because the explosion shock wave cannot kick all the deposited rock dust up when the deposited rock dust amount reaches a certain value, thus reducing the explosion suppression effect. The explosion pressure curves of 30 kg/m^3 and 36 kg/m^3 largely coincide, which shows that 36 kg/m^3 is basically the upper limit of the deposited dust rising by the shock wave. The maximum explosion pressure for the amount of 36 kg/m^3 decreases by 40% compared with that without inert rock dust, which greatly reduces the damage degree. According to the Bowen damage curve [36], no human can survive when suffering a pressure over 1 bar. Mark a horizontal line corresponding to the critical overpressure 1 bar in Fig. 7, intersect each overpressure curve with it, then make a vertical line from the intersection to the cross axis to obtain the “death” zone. For the amounts of 12 kg/m^3, 24 kg/m^3, 30 kg/m^3, 36 kg/m^3, 45 kg/m^3, the “death” zones are 338.4 m, 262.5 m, 235.3 m, 230 m and 249.4 m long, which are respectively 12.08, 9.38, 8.40, 8.21 and

8.91 times the length of the premixed gas section (28 m).

3.2. Temperature distribution in pipeline

Fig. 8a shows the temperature distribution with time under the deposited rock dust amount of 24 kg/m^3. It can be seen that the flame has contact with the rock dust cloud at 0.138 s, and the highest temperature of the flame front is 2600 K. The temperature gradient of the flame front increases when the flame reaches the inert dust cloud, then the heat dissipation rate increases, resulting in the flame temperature decreasing gradually. Meanwhile, part of the inert dust cloud is heated at a temperature of approximately 1000 K after 0.618 s. From 1.325 s to 1.585 s, the overall temperature of the flame continues to decrease, indicating that no reactive heat is produced, which implies the flame to be extinguished. When the amounts are 18 kg/m^3, 30 kg/m^3, 36 kg/m^3 and 45 kg/m^3, the temperature distributions are similar to those shown in Fig. 8a.

Fig. 8b shows the temperature distribution with time under the amount of 12 kg/m^3. It is shown that the temperature gradually falls, and then rises again. After 0.305 s, the temperature of the flame front rises to 2400 K, indicating that the gas explosion in the pipeline begins to develop again. The temperature distribution under the amount of 7 kg/m^3 is similar to Fig. 8b.

The temperature along the pipeline for different rock dust amounts is illustrated in Fig. 9. A consistent trend reflected is that the peak temperature decreases with the increase of rock dust amount. The heat absorption capacity of dust cloud is saturated when the deposited rock dust amount is 36 kg/m^3.

3.3. Flame speed

It can be seen from Fig. 10 that the dispersed inert rock dust cloud in the pipeline can effectively suppress the explosion flame propagation and reduce the flame speed. Compared to the peak flame speed of premixed gas explosion (700 m/s), the peak value at the deposited rock dust amount of 36 kg/m^3 is reduced by half. When the amount of deposited rock dust is 12 kg/m^3, the flame speed appears to increase a little in the process of descent, and the spread range is not changed notably compared to the gas explosion. The spread range and the peak flame speed decrease with the increase of the deposited rock dust amount, but the suppression is less effective when the amount reaches 45 kg/m^3.

It is to note that the flame speed has a sharp drop after reaching the peak value in Fig.10. In order to find the effective range of the raised dust concentrations to suppress explosion, the slopes of the downward section of the curve are obtained and compared. The dust concentration corresponding to the maximum reduction of the flame

speed namely corresponding to the maximal slope's absolute value is taken as the effective raised dust concentration. The effective concentrations for different deposited rock dust amounts are obtained and shown in Fig. 11. Based on the curve, the range of raised rock dust concentrations to suppress explosion effectively is 2.5-3.5 kg/m^3.

3.4. Combustion rate distribution

The combustion rate along the pipeline axis for gas explosion is shown in Fig. 12. The peak combustion rates increase as the flame propagating along the pipeline until achieving the highest value beyond the original premixed region (28 m), and then decreases gradually. The time of flame arrival at a point is assumed to correspond to the time of the maximum combustion rate attained [37], so the flame length of the gas explosion (L_0) is 120 m. When the deposited rock dust amount is 36 kg/m^3, the flame length is shortened to 70 m as deduced from Fig. 13. This is because the raised rock dust in the area ahead of the flame hinders the diffusion of unburned gas to the no-methane-occupied region, and the explosion gets weaker as a result of the reduction of the gas concentration, and the combustion rates drops accordingly. Similar plots were obtained by plotting the peak combustion rate along the pipeline at different deposited rock dust amounts, as shown in Fig. 14. All curves appear to rise to a maximum and then fall to a very low value. As the amount of rock dust increases, the curve drops more quickly, but the trend goes into reverse with the amount rising from 36 kg/m^3 to 45 kg/m^3.

The ratios of the flame lengths under different deposited rock dust amounts to L_0 are illustrated in Fig. 15. It is clearly shown that the setting of the inert rock dust layer can shorten the flame length and the largest shortened length reaches 42%, which can alleviate the harm caused by high-temperature flame effectively. It should be noted that the flame length increases instead of decreasing with the amount rising from 36 kg/m^3 to 45 kg/m^3, and it is illustrated that there is an upper limit for the amount of deposited rock dust.

4. Conclusion

A numerical study on gas explosion suppression by the deposited inert rock dust is undertaken. The propagation of premixed gas explosion suppressed by deposited inert rock dust layer in a large length-diameter ratio (148.5:1) pipeline is modeled with the standard k-ε model and the discrete phase model, and the numerical model is well validated by the experiments under similar conditions. Under the deposited rock dust amounts of 7 kg/m^3, 12 kg/m^3, 18 kg/m^3, 24 kg/m^3, 30 kg/m^3, 36 kg/m^3 and 45 kg/m^3, the conclusions can be drawn from the simulation results as follows.

The rock dust rising induced by premixed explosion shock wave can form a barrier in the pipeline to suppress explosion, and the range of raised dust concentrations to suppress explosion effectively is 2.5-3.5 kg/m^3.

The change trend of the overpressure with the deposited rock dust amount is consistent with that of the temperature, the flame speed and the flame length, and the trends illustrate that only a greater amount of deposited rock dust within a certain range can enhance the ability for explosion attenuation.

When the rock dust amount is less than 12 kg/m^3, the explosive grows again after passing through the rock dust suppression zone, that is to say, it cannot be completely suppressed. When the amount is more than 45 kg/m^3, the effects of explosion suppression begin to weaken.

The effects of explosion suppression by deposited inert rock dust are: the overpressure is reduced by 40%, the peak flame speed by 50%, and the flame length by 42% respectively, compared with those of the gas explosion for stoichiometric mixture (with methane concentration of 9.5%).

Acknowledgments

The research presents in this paper was supported by the National Science Foundation of China (11772057).

References

[1] P. Kosinski, A.C. Hoffmann, An investigation of the consequences of primary dust explosions in interconnected vessels, J. Hazard. Mater. 137(2006) 752–761.

[2] Y. Liu, X.T. Liu, X.Q. Li, Numerical investigation of hydrogen detonation suppression with inert particle in pipelines, Int. J. Hydrogen Energy. 41 (2016) 21548-21563.

[3] M. Gieras, R. Klemens, Effectiveness of an active dust and gas explosion suppression system, J. Power Technol. 92 (2012) 1–11.

[4] Y. Wang, Y.S. Cheng, M.G Yu, Y. Li, J.L. Gao, L.G. Zheng, H.W. Yi, Methane explosion suppression characteristics based on the NaHCO3 /red-mud composite powders with core-shell structure, J. Hazard. Mater. 335 (2017) 84–91.

[5] X.F. Chen, Y. Zhang, Q.M. Zhang, S.F. Ren, J.X. Wu, Experimental investigation on micro–dynamic behavior of gas explosion suppression with SiO2 fine powder, Theor. Appl. Mechanic. Lett. 14 (2011) 1–4.

[6] J. Amrogowicz, W. Kordylewskiw, Effectiveness of dust explosion suppression by carbonates and phosphates, Combust. Flame. 85 (1991) 520–522.

[7] H. Spath, A.S. Yu, N. Dewen, A new dimension in coal mine safety: explospot, active explosion suppression

technology, Procedia Eng. 26 (2011) 2191–2198.

[8] B. Hjertager, Three-dimensional Modeling of Flow, Heat Transfer, and Combustion. In: Handbook of Heat and Mass Transfer. Gulf Publishing, Houston, 1986, pp.1303-1350.

[9] T. Skjold, D. Castellanos, K.L. Olsen, R.K. Eckhoff, Experimental and numerical investigation of constant volume dust and gas explosions in a 3.6-m flame acceleration tube, J. Loss Prev. Process Ind. 30(2014) 164-176.

[10] A. Tascón, P.J. Aguado, Simulations of vented dust explosions in a 5 m3 vessel, Powder Technol. 321(2017) 409–418.

[11] G. Ferrara, A. Di Benedetto, E. Salzano, G. Russo. CFD analysis of gas explosions vented through relief pipes, J. Hazard. Mater. 137 (2006) 654–665.

[12] A.V. Fedorov, I.A. Fedorchenko, Computation of dust lifting behind a shock wave sliding along the layer. Verification of the model, Combusti. Explo. Shock+ 41(2005), 336–345.

[13] R. Klemens, P. Kosinski, P. Wolanski, V.P. Korobeinikov, V.V. Markov, I.S. Menshov, I.V. Semenov, Numerical study of dust lifting in a channel with vertical obstacles, J. Loss Prev. Process Ind. 14(2001) 469–473.

[14] A. Di Benedetto, P. Russo, R. Sanchirico, V. Di Sarli, , CFD simulations of turbulent fluid flow and dust dispersion in the 20 liter explosion vessel, AIChE 59 (2013) 2485–2496.

[15] P. Kosinski, Numerical investigation of explosion suppression by inert particles in straight duct, J. Hazard. Mater. 154 (2008) 981–991.

[16] P. Oleszczak, R. Klemens, Mathematical modelling of dust–air mixture explosion suppression, J. Loss Prev. Process Ind.19 (2006) 187–193.

[17] M. Krasnyansky, Prevention and suppression of explosions in gas–air and dust–air mixtures using powder aerosol–inhibitor, J. Loss Prev. Process Ind.19 (2006) 729–735.

[18] R. Klemens, B. Szatan, M. Gieras, P. Wolańskia, A. Marandab, J. Nowaczewskib, J. Paszulab, Suppression of dust explosions by means of different explosive charges, J. Loss Prev. Process Ind.13 (2000) 265–275. · ·

[19] J.E. Going, K. Chatrathi, K.L. Cashdollar, Flammability limit measurements for dusts in 20-L and 1-m3 vessels, J. Loss Prev. Process Ind. 13 (2000), 209–219.

[20] A.G. Dastidar , P.R. Amyotte , J. Going, K. Chatrathi, Inerting of coal dust explosions in laboratory and intermediate scale chambers, Fuel, 80 (2001)1593–1602.

[21] Y. Shoshin, G. Gorecki, J. Jarosinski, T. Fodemski, Experimental study of limit lean methane/air flame in a standard flammability tube using particle image velocimetry method, Combust. Flame. 57 (2010) 884–892.

[22] C.G. Ilea, P. Kosinski, A.C. Hoffmann, Three-dimensional simulation of a dust lifting process with varying parameters, Int. J. Multiphas. Flow. 34 (2008) 869–878.

[23] P. Kosinski, A.C. Hoffmann, R. Klemens, Dust lifting behind shock waves: comparison of two modelling techniques, Chem. Eng. Sci. 60 (2005) 5219–5230.

[24] Fluent Inc, Fluent release 6.3 user guide, Fluent Inc., 2006.

[25] B.E. Launder, D.B. Spalding, Lectures in Mathematical Models of Turbulence, Academic Press, London, 1972.

[26] B.F. Magnussen, B.H. Hjertager, On mathematical models of turbulent combustion with special emphasis on soot formation and combustion. In 16th Symp.(Int'l.) on Combustion. The Combustion Institute, 1976.

[27] P.R. Amyotte, Solid intertants and their use in dust explosion prevention and mitigation, J. Loss Prev. Process Ind. 19 (2006) 161–173.

[28] Q.M. Liu, Y.L. Hu, C.H Bai, M. Chen, Methane/coal dust/air explosions and their suppression by solid particle suppressing agents in a large-scale experimental tube, J. Loss Prev. Process Ind. 26 (2013) 310–316.

[29] Q.Q. Huang, R. Honaker, Optimized reagent dosage effect on rock dust to enhance rock dust dispersion and explosion mitigation in underground coal mines, Powder Technol. 301 (2016) 1193–1200.

[30] State Administration of Work Safety, Coal Mine Safety Regulation, China, 2016.

[31] J.D. Xu, S.L. Xu, G.Y. Yang, Experimental study on mine gas explosion diffusion, J. China Coal Soc. 32 (2004) 55–57.

[32] Q. Wang, Z.W. Shen, Z.R Guo, Influences of nonmetallic powders on premixed methane-air flame propagation in square tube, Expl. Shock Waves. 33 (2013) 359–362.

[33] M.M. Kopp, N.S. Donato, E.L. Petersen, W.K. Metcalfe, Z. Serinyel, H.J. Curran, Ignition and oxidation of ethylene–air mixtures at elevated pressures. In: AIAA Aerosp. Sci. Meet.Incl. New Horiz. Forum Aerosp. Expos, Orlando, US, 2010.

[34] Q. Zhang, L. Pang, Numerical analysis of characteristics of wind caused by methane-air explosion, Eng. Comput. 31 (2014) 490–500.

[35] G. Dong, B. Fan, B. Xie, J.F. Ye, Experimental investigation and numerical validation of explosion suppression by inert particles in large scale duct, P. Combust. Inst. 30 (2005) 2361–2368.

[36] I.G. Bowen, E.R. Flecther, D.R. Richmond, F.G. Hirsch, C.S. White, Biophysical mechanisms and scaling procedures applicable in accessing responses of the thorax energized by air-blast overpressures or by nonpenetrating missiles, Ann. N. Y. Acad. Sci. 152 (1968) 122–146.

[37] Q.J. Ma, Q. Zhang, L. Pang, Hazard effects of high-speed flow from methane-hydrogen premixed explosions,

Process Saf. Prog. 33 (2014) 85–93.

Figures captions

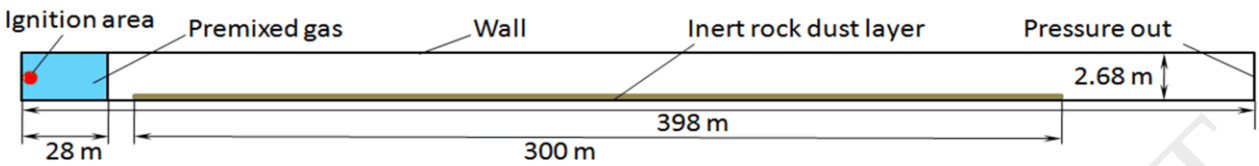

Fig. 1. Sketch of the physical model.

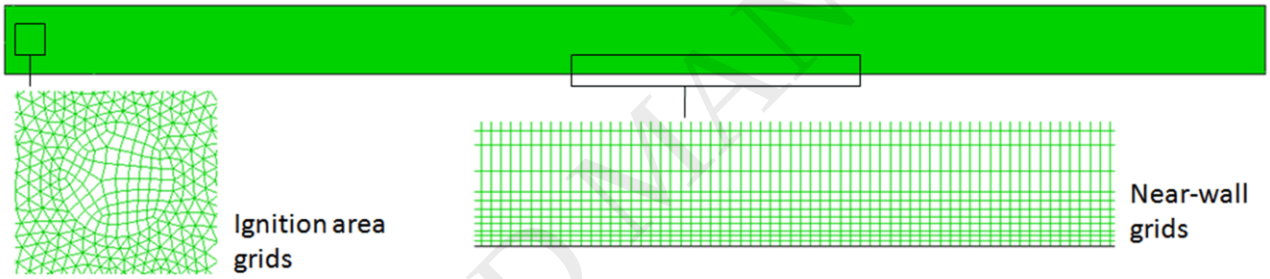

Fig. 2. The mesh generation.

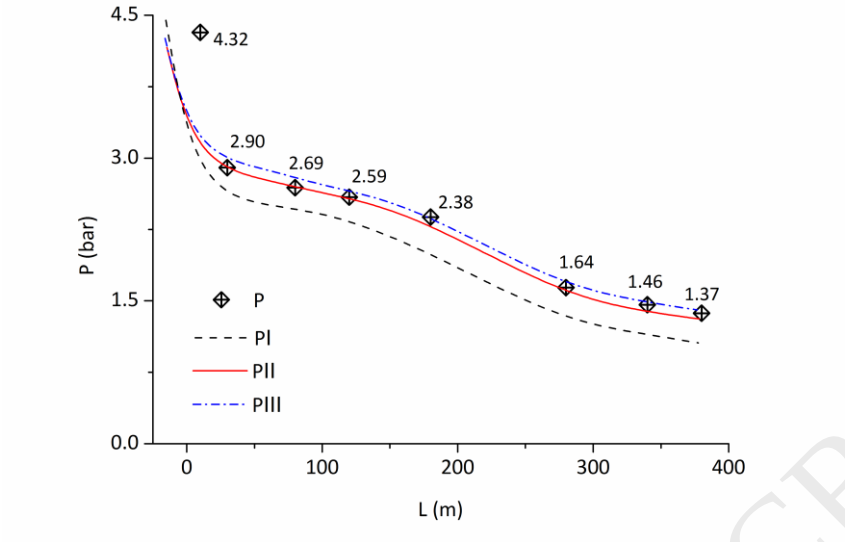

Fig. 3. Experimental pressures and simulation results.

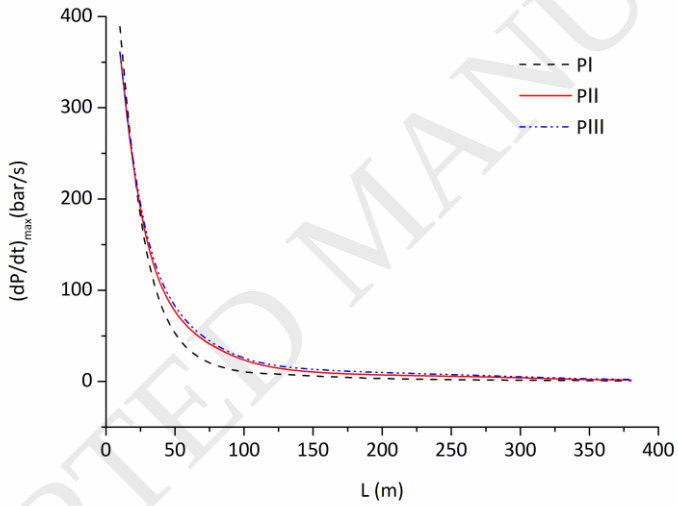

Fig. 4. The maximum rates of pressure rise along the pipeline under three models.

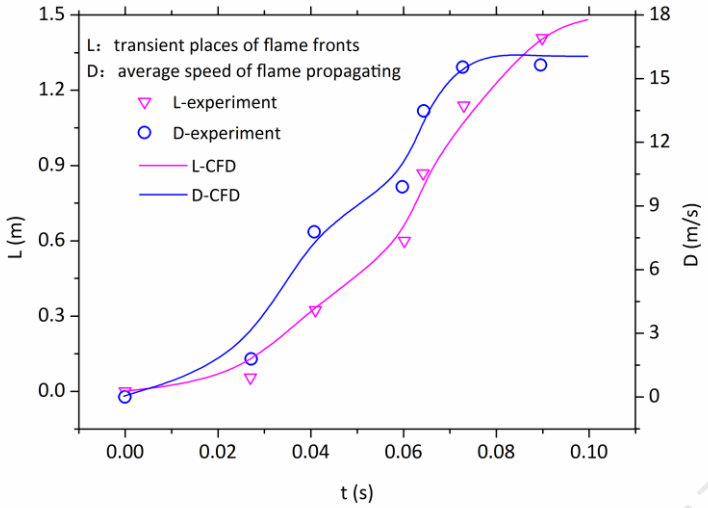

Fig. 5. Comparison between measured flame propagation values and simulation results.

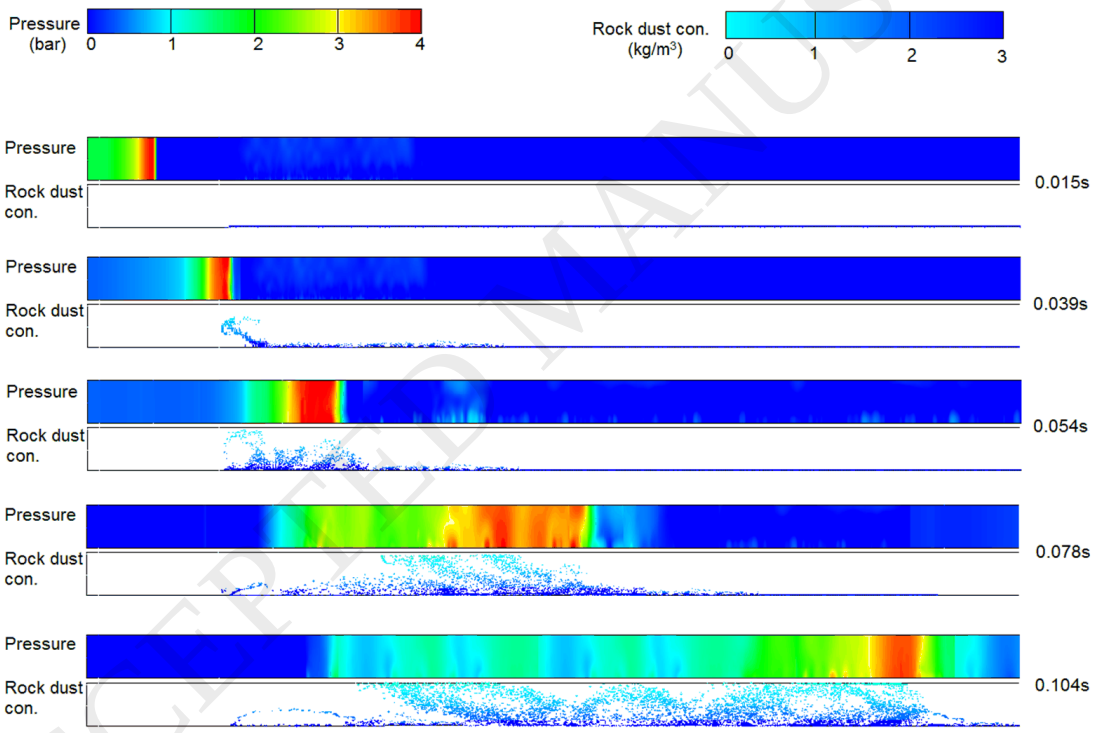

Fig. 6. The process of deposited rock dust rising induced by explosion shock wave.

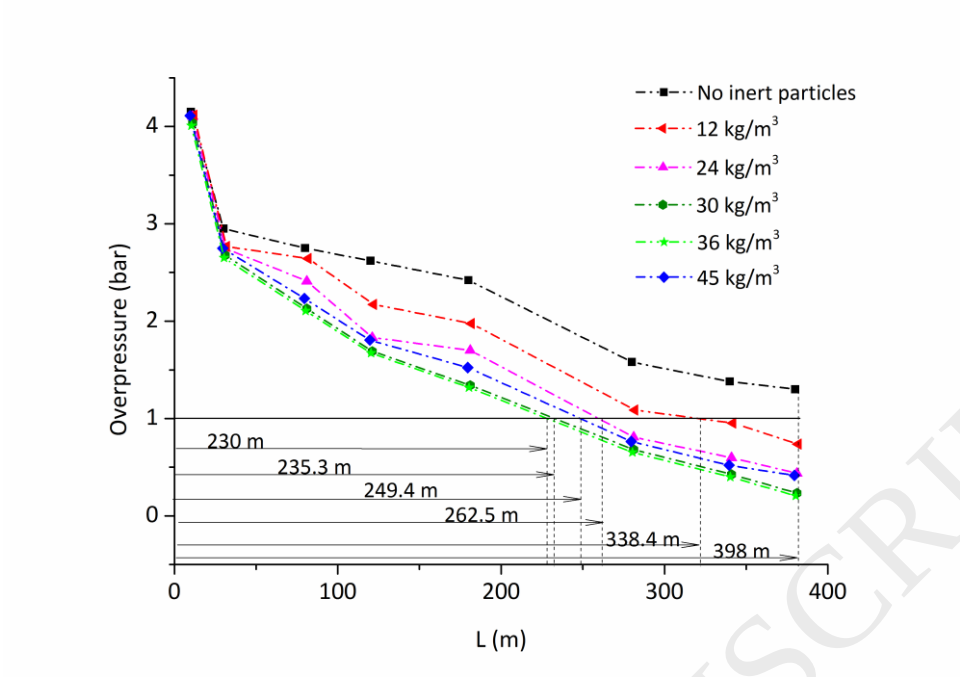

Fig. 7. Peak overpressure along the pipeline at different deposited rock dust amounts.

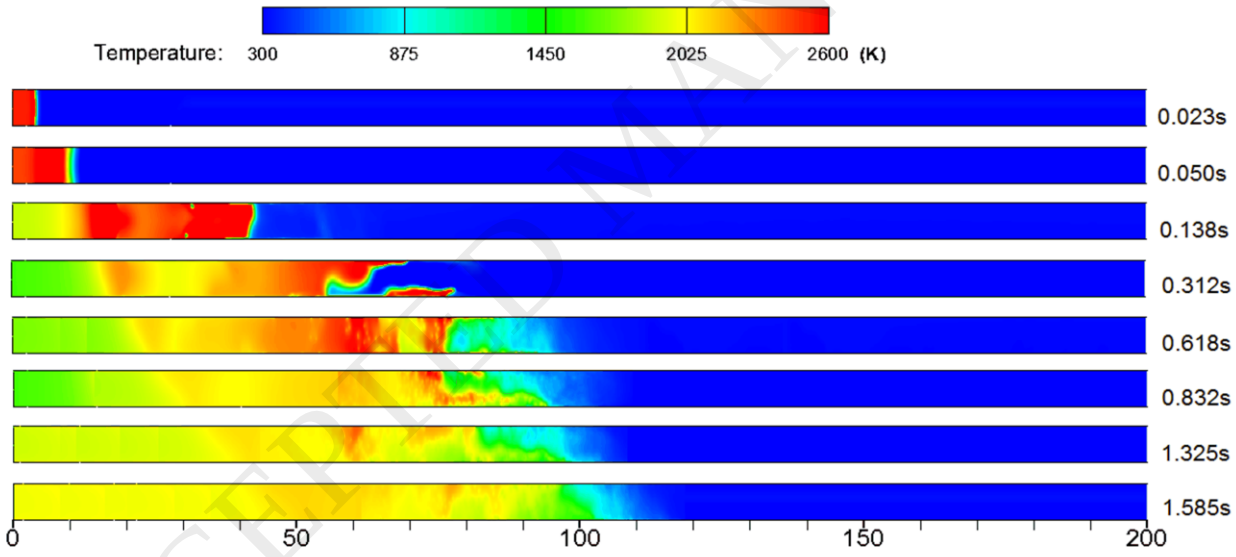

a. 24 kg/m^3

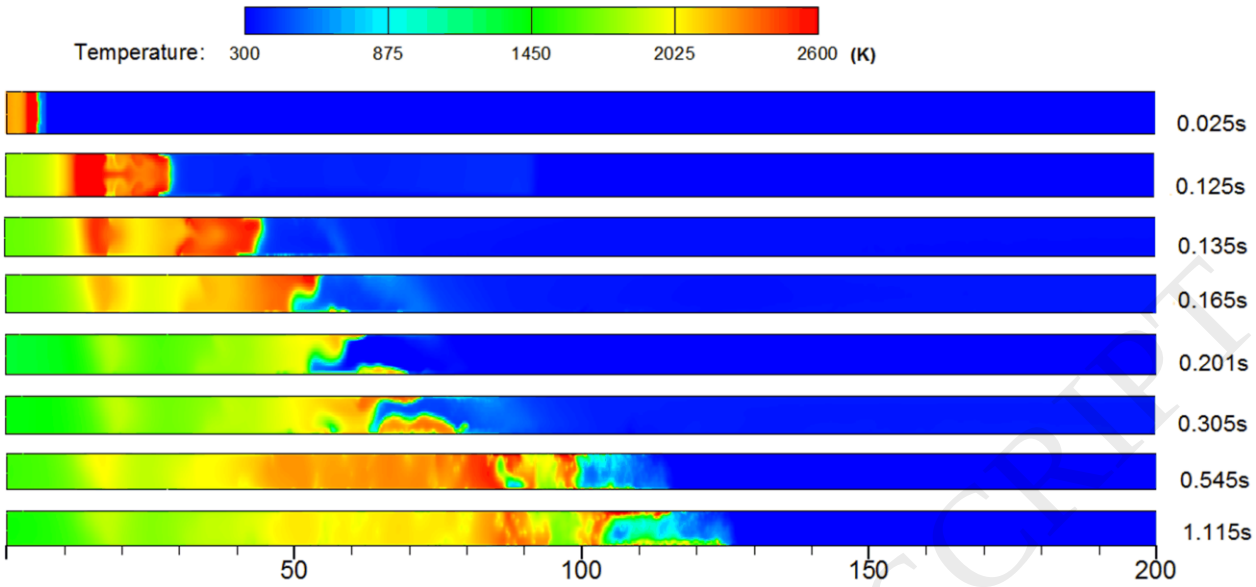

b. 12 kg/m^3

Fig. 8. Temperature distribution in pipeline at different deposited rock dust amounts.

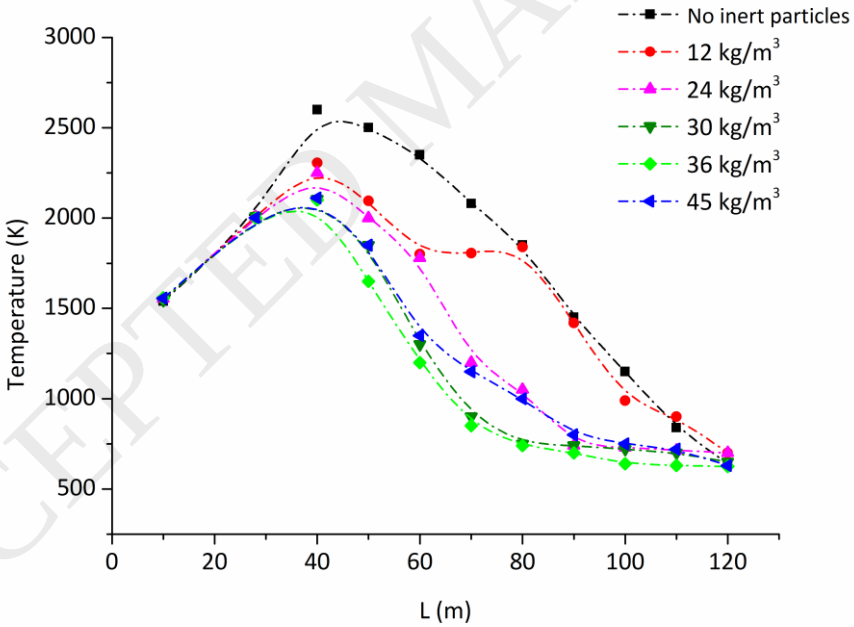

Fig. 9. Temperature along the pipeline at different deposited rock dust amounts.

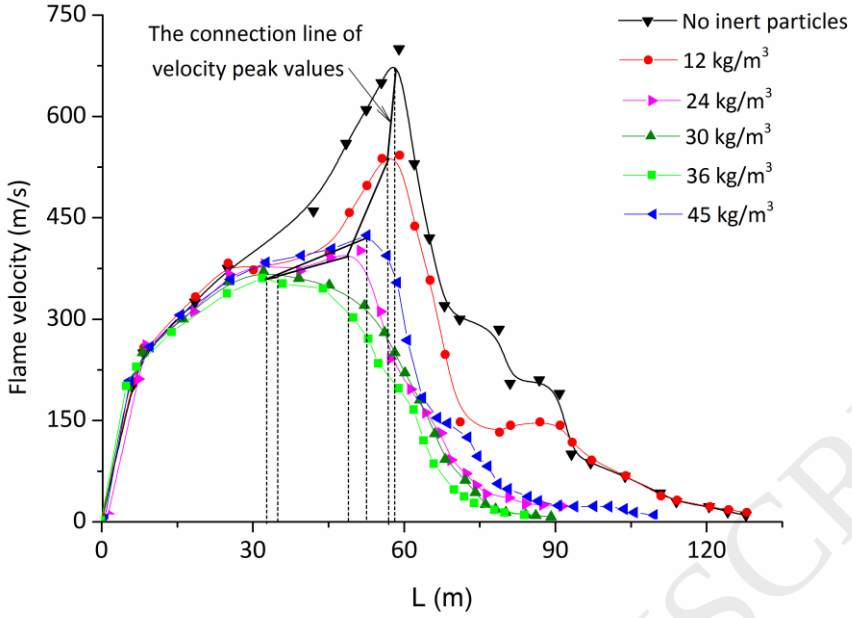

Fig. 10. Flame speed along pipeline at different deposited rock dust amounts.

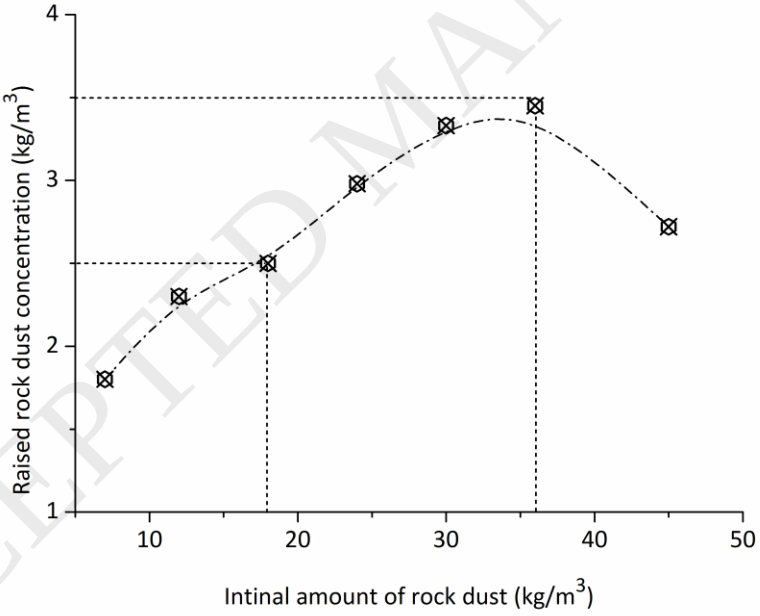

Fig. 11. The effective raised dust concentrations at different deposited rock dust amounts.

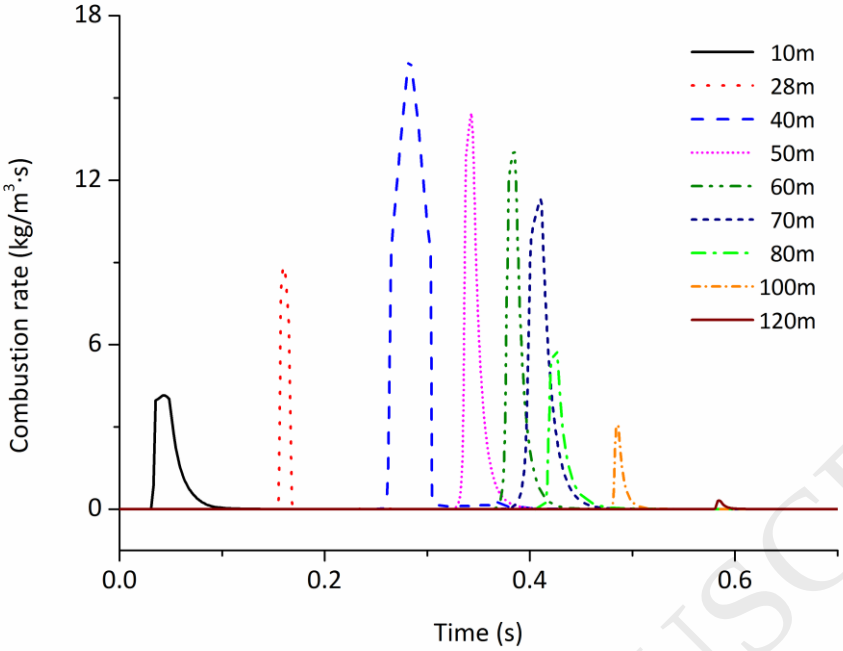

Fig. 12. Combustion rate time histories at various locations along the pipeline of gas explosion.

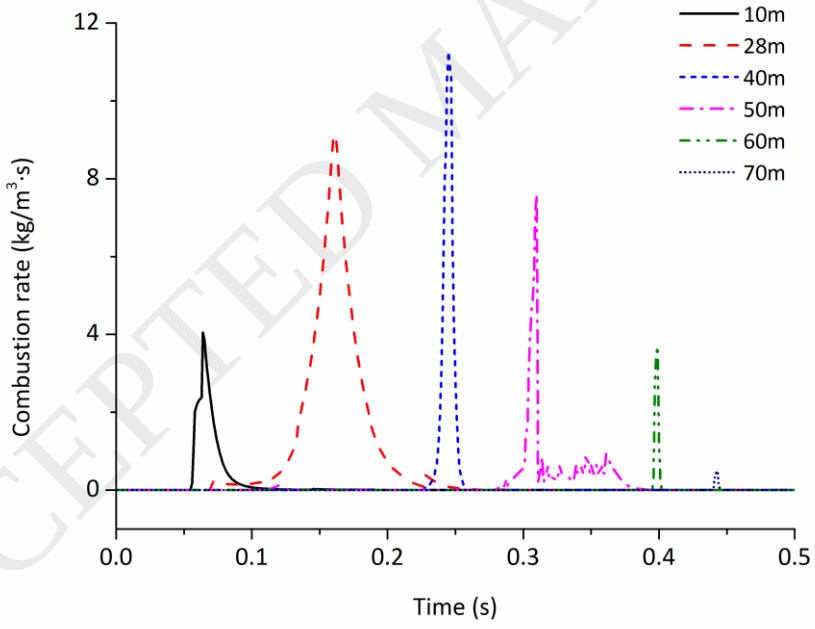

Fig. 13. Combustion rate time histories at various locations at the deposited rock dust amount of 36 kg/m^3.

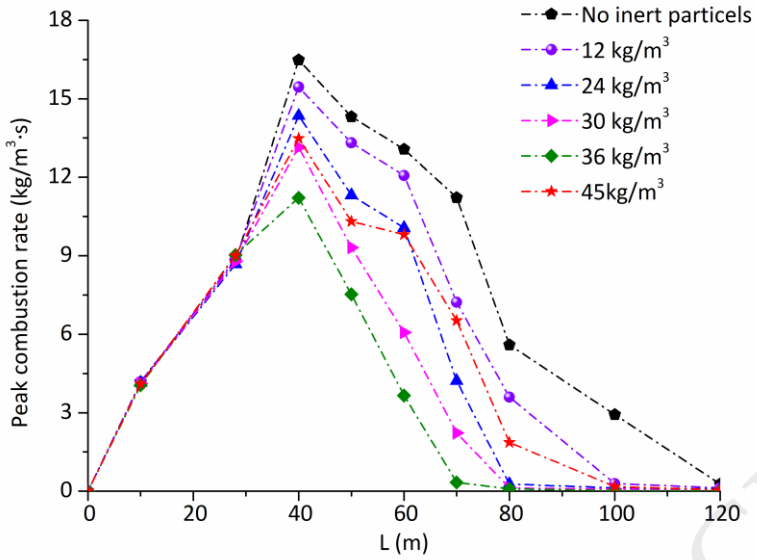

Fig. 14. Peak combustion rate along pipeline at different deposited rock dust amounts.

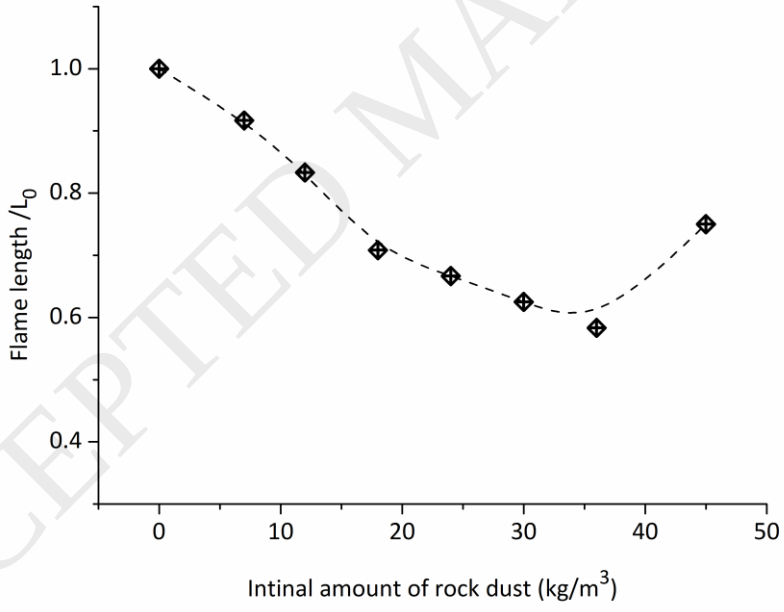

Fig. 15. Flame lengths at different deposited rock dust amounts.

Tables

Table 1

Size distribution of the inert particles.

Size/μm	5	15	25	45	50	60	75	80	100
Mass percentage less than	2.35	18.85	39.72	52.32	68.45	77.45	83.54	93.35	100

Table 2

Constant parameters.

Parameter	Value
Pipeline length	398 m
Pipeline diameter	2.68 m
Length of the premixed gas section	28 m
CH_4 volume content in the premixed gas	9.5 %
Length of the inert particles layer	300 m
Initial pressure and temperature	1 bar, 300 K
Particle density	2800 kg/m^3
Mean particle diameter (D_{50})	41.32 μm

Table 3

Mesh models

Model	Grid Number
Model Ⅰ	106 200
Model Ⅱ	584 800
Model Ⅲ	1 154 400